

THE EARLY EVOLUTION OF PRIMORDIAL PAIR-INSTABILITY SUPERNOVAE

C.C. JOGGERST^{1,2} AND DANIEL J. WHALEN³

Draft version August 15, 2018

ABSTRACT

The observational signatures of the first cosmic explosions and their chemical imprint on second-generation stars both crucially depend on how heavy elements mix within the star at the earliest stages of the blast. We present numerical simulations of the early evolution of Population III pair-instability supernovae with the new adaptive mesh refinement code CASTRO. In stark contrast to 15 - 40 M_{\odot} core-collapse primordial supernovae, we find no mixing in most 150 - 250 M_{\odot} pair-instability supernovae out to times well after breakout from the surface of the star. This may be the key to determining the mass of the progenitor of a primeval supernova, because vigorous mixing will cause emission lines from heavy metals such as Fe and Ni to appear much sooner in the light curves of core-collapse supernovae than in those of pair-instability explosions. Our results also imply that unlike low-mass Pop III supernovae, whose collective metal yields can be directly compared to the chemical abundances of extremely metal-poor stars, further detailed numerical simulations will be required to determine the nucleosynthetic imprint of very massive Pop III stars on their direct descendants.

Subject headings:

1. INTRODUCTION

The first stars in the universe form at $z \sim 20$ and are likely very massive, 30 - 500 M_{\odot} (Bromm et al. 1999; Abel et al. 2000, 2002; Bromm et al. 2002; Nakamura & Umemura 2001; O’Shea & Norman 2007). The fates of these stars depend on their masses: 15 - 50 M_{\odot} stars die in core collapse supernovae (CC SNe), 140 - 260 M_{\odot} stars explode in far more energetic thermonuclear pair-instability supernovae (PISNe Heger & Woosley 2002), and 40 - 60 M_{\odot} stars may die as hypernovae, whose explosion mechanisms are not yet understood but are thought to have energies intermediate to those of CC and pair-instability SNe (Iwamoto et al. 2005). Most Pop III SNe (Bromm et al. 2003; Kitayama & Yoshida 2005; Greif et al. 2007) occur in low densities ($0.1 - 1 \text{ cm}^{-3}$) because UV radiation from the star sweeps most of the baryons from the dark matter halo in which it resides (Whalen et al. 2004; Kitayama et al. 2004; Alvarez et al. 2006; Abel et al. 2007; Wise & Abel 2008a).

Metals from Pop III SNe determine the character of second-generation stars and the primeval galaxies they populate by enhancing cooling in the gas in which such stars form, and therefore the mass scales on which it fragments. The manner in which the first metals contaminate pristine gas in the primordial IGM crucially depends on mixing processes that have only begun to be studied numerically. Preliminary calculations indicate that metals from Pop III SNe mix with gas in a halo on two characteristic spatial scales prior to their emergence into cosmological flows on kpc scales (Whalen et al. 2008): 10 - 15 pc, when a reverse shock forms in the remnant,

and 150 - 200 pc, when the remnant collides with the dense shell of the relic H II region of the progenitor. New simulations now prove that violent mixing can occur *within* the star prior to shock breakout from its surface, if the star is 15 - 40 M_{\odot} (Joggerst et al. 2010a, hereafter JET10). Capturing mixing on the smallest scales is prerequisite to following its cascade out to the largest ones, and hence to determining the colors and morphologies of primitive galaxies. Early mixing also governs which elements are imprinted on next-generation stars, whose chemical abundances may impose indirect constraints on the masses of the stars that enriched them. Low-mass remnants of this generation are now sought in ongoing surveys of ancient, dim metal-poor stars in the Galactic halo (Beers & Christlieb 2005; Frebel et al. 2005). Since mixing in Pop III SNe in part sets elemental abundances in second-generation stars, it is integral to future measures of the primordial IMF.

Early mixing is also key to computing the light curves and spectra of the first cosmic explosions, whose detection could yield the first *direct* measure of the primordial IMF. Optical and UV radiation breaks free of the SN shock when the ejecta reaches the outer envelope of the star and is exposed to the IGM. In the frame of the shock, the photosphere from which photons escape into space descends deeper into the ejecta as it expands outward because of the spherical dilution of the ejecta. If mixing precedes radiation breakout, it determines the elements that the photosphere encounters as it sinks deeper into the ejecta, and therefore the emission lines that propagate into the IGM over time. Accurate multidimensional models of the explosion from its earliest stages are therefore necessary to compute lines in primordial SN light curves and spectra.

Mixing in galactic core-collapse supernovae has been studied for over twenty years, particularly in connection with SN 1987A (e.g. Fryer et al. 2007, and references therein). A core objective of these studies is to understand the premature appearance of ^{56}Ni in the spectra of 1987A, whose emission lines appear much earlier than

¹ Department of Astronomy and Astrophysics, University of California at Santa Cruz, Santa Cruz, CA 95060. Email: cchurch@ucolick.org

² Nuclear and Particle Physics, Theoretical Astrophysics and Cosmology (T-2), Los Alamos National Laboratory, Los Alamos, NM 87545

³ McWilliams Fellow, Department of Physics, Carnegie Mellon University, Pittsburgh, PA 15213

a simple picture of segregated, spherically-symmetric expanding mass shells would predict. Mixing in Pop III core-collapse SNe was first examined by Joggerst et al. (2009), who found that both vigorous mixing and fallback onto the compact remnant in 15 - 40 M_{\odot} Pop III SNe govern which metals escape into the IGM at high redshifts.

PISNe may have been commonplace in the primeval universe, but their enrichment of the early IGM is yet to be understood. To investigate the propagation of metals into the IGM by such explosions, constrain their nucleosynthetic imprint on second-generation stars, and to evaluate the impact of mixing on PISN spectra, we have performed two-dimensional simulations of the explosions of 150 - 250 M_{\odot} stars. In § 2 we review how blast profiles from the KEPLER code were ported as initial conditions to CASTRO and discuss what factors govern the presupernova structure of the star. We examine the outcomes of the explosions in § 3 and in § 4 we conclude.

2. MODELS

2.1. KEPLER

As in JET10, the simulations in our PISN survey were carried out in two stages. First, primordial stars were evolved through all stages of stable nuclear burning from the zero-age main sequence to initial collapse via the pair instability in the one-dimensional Lagrangian stellar evolution code KEPLER (Weaver et al. 1978; Woosley et al. 2002). The PISN is triggered when this collapse incites explosive O, and some cases Si, burning. Unlike the simulations of JET10, in which the blast is artificially launched with a piston, the pair instability and subsequent collapse that triggers these explosions are an emergent feature of the stellar evolution calculation. They are genuinely spherical, barring (magneto)rotational effects, and their energies are set by O and Si burning. The blast was followed until the end of all nuclear burning, ~ 20 s after the start of the explosion. The energy generated was computed with a 19-isotope network up to the point of oxygen depletion in the core of the star and with a 128-isotope quasi-equilibrium network thereafter.

2.2. CASTRO

The one-dimensional explosion profiles were then mapped onto two-dimensional RZ axisymmetric grids in CASTRO (Compressible ASTROphysics), a multi-dimensional Eulerian AMR code with a high-order unsplit Godunov hydro solver (Almgren et al. 2010). Each explosion was evolved past breakout from the surface of the star until all mixing ceased and each element in the ejecta was expanding homologously in mass coordinate. We smoothly join the density at the surface of the star to a uniform circumstellar medium of 1 cm^{-3} with an $r^{-3.1}$ power law, in keeping with the usual assumption of a low-density H II region around the progenitor star with no wind-blown shell or prior mass ejection. The medium beyond the star has no effect on the dynamics within the star if its density falls more steeply than r^{-3} . In mapping the radial profile onto the RZ grid in CASTRO, care was taken to resolve the key elements of the explosion: the shock, the shells of elements, and the high-density core. In particular, both the ^{56}Ni core and the O shell were resolved with a minimum of 16 cells. Our mapping excludes

departures from spherical symmetry due to O burning, but such perturbations would likely be high mode and low amplitude and therefore have minimal effect on the evolution of instabilities. Our models thus only capture later asymmetries of mode greater than $l = 1$ or 2.

As in JET10, we adopt a monopole approximation for self-gravity. We first compute a radial average of the density from the RZ grid to create a one-dimensional density profile. We then compute a one-dimensional gravitational potential from this profile and map it back onto the RZ grid. Since departures from spherical symmetry in the densities are minor, this approximation has a negligible effect on the final state of the explosion. Because the PISN completely disperses the star, there is no compact remnant, fallback, or thus any need to include a point potential centered at the origin of the coordinate mesh.

We follow 15 chemical elements as individual species, each with their own continuity equation, and calculate local energy deposition due to radioactive decay of ^{56}Ni in the same manner as JET10. However, the formation of a nearly degenerate core at white dwarf densities in the progenitor necessitates the use of the Helmholtz equation of state (EOS) at early stages of the explosion. As the ejecta expands and cools, we transition back to the ideal EOS used in JET10, which assumes that the gas is fully ionized and includes contributions from both radiation and ideal gas pressure.

The base grid is 1024^2 , with the initial outer boundaries set so that the inner portion of the star is resolved as described above using no more than 6 levels of refinement. The star is centered at the lower left corner of the mesh. We apply reflecting and outflow boundary conditions to the inner and outer boundaries of the grid, respectively. Our refinement criteria are the same as those in JET10. When the shock nears the edge of the grid, the simulation is stopped, the grid is doubled, and the calculation is then restarted, subtracting or adding levels of refinement as needed. This procedure is repeated up to 12 times, depending on the model. We halt the simulation when all chemical species are expanding homologously, which always occurs by the time the ejecta has propagated a short distance into the uniform circumstellar density.

2.3. Progenitor Models

JET10 found that mixing in low-mass Pop III core-collapse explosions primarily depends on the internal structure of the progenitor. We likewise expect the early evolution of pair-production explosions to be determined by the envelope of the star, which is determined its mass, internal convective mixing over its lifetime, and by its metallicity. Capturing the full range of structures for these stars is essential to a comprehensive survey of early mixing in Pop III supernovae.

2.3.1. Convective Mixing

The initial absence of metals and the large contribution of radiation to the pressure in massive Pop III stars promotes convection within them. The CNO cycle cannot begin in primordial stars until a threshold mass fraction of ^{12}C is first created by the triple α process. This trace ^{12}C sets the entropy of the hydrogen layer to be just above that in the core, without the sharp entropy

TABLE 1
PISNE MODELS: PROPERTIES AT TIME MODELS WERE MAPPED TO 2D

model	M_{He} (M_{\odot})	M_N (M_{\odot})	M_{56Ni} (M_{\odot})	M_{final} (M_{\odot})	R (10^{13} cm)	E_{kin} (10^{51} ergs)
u150	41	9.1(-5)	0.079	143	16	3.7
u175	46	1.1(-4)	0.72	164	18	9.5
u200	50	1.3(-4)	5.2	183	19	17
u225	54	1.1(-3)	17	200	33	28
u250	68	1.7(-4)	38	238	23	34
z175	53	1.6(-5)	0.24	175	4.2	4.7
z200	60	1.8(-5)	2.0	200	4.5	12
z225	67	1.7(-5)	8.8	225	4.9	17
z250	74	1.6(-5)	23	250	6.2	29

gradient in the upper layer of the helium shell that is usually present in He burning stars with metals. This plus radiation pressure facilitates convection. In 140 - 260 M_{\odot} stars, the central convection zone can approach, come in contact with, or even reach into the lower hydrogen layers, mixing them with carbon brought up from the core during helium burning. When these two high-temperature components mix, they burn vigorously, elevating energy release rates in the H shell by up to several orders of magnitude (the so-called hydrogen boost).

Convection affects the structure of the star in two ways. First, since it raises energy production (and hence opacities) in the lower hydrogen layers, the star can puff up by more than an order of magnitude in radius and acquire a red supergiant structure. Second, if convection is extreme the transport of material out of the core could reduce its size and explosion energy in comparison to modest convection. Unfortunately, one-dimensional stellar evolution models cannot predict these inherently three-dimensional processes from first principles. Instead, they parametrize them with semi-convection coefficients.

2.3.2. Metallicity

Gas in high-redshift halos that is enriched to metallicities below $10^{-3.5} Z_{\odot}$ fragments on mass scales that are essentially identical to those of pristine gas and still forms very massive stars (e. g. Bromm et al. 2001; Mackey et al. 2003; Smith & Sigurdsson 2007). However, such small metal fractions are more than enough to enhance CNO reaction and energy generation rates in the hydrogen burning layers of the star, enlarging it in the same manner as convective mixing (Hirschi 2007; Ekström et al. 2008). Hence, we would expect a strong degeneracy between the influence of metals and convection on the envelope of the star, and that the full range of mixing in PISNe can be as easily spanned by metallicity as by convective overshoot.

We considered 150, 175, 200, 225 and 250 M_{\odot} non-rotating progenitors at $Z = 0$ (the z-series) and $Z = 10^{-4} Z_{\odot}$ (the u-series), which we summarize in Table 1. The $Z = 0$ 150 M_{\odot} star collapses to a black hole without exploding, so we exclude it from our CASTRO models. We employ metallicity rather than convective overshoot to cover the range of plausible progenitor structures in our study, because there is uncertainty about how much semi-convection there is in a given star but none about the range of metallicities over which it can form ($Z = 0$ and 10^{-4}). Comparison of Table 1 with Table 1 of Scannapieco et al. (2005) confirms that for a given progenitor mass these two metallicities do yield upper and

lower limits to stellar radius similar to those for all reasonable values of semi-convection coefficients.

3. RESULTS

As expected, the u-series models die as red giants, with radii more than an order of magnitude larger than those of the z-series, which die as blue giants. As shown in Table 1, the u-series models in general have more energetic explosions than the z-series models for a given mass. As we show in Figure 1, convective mixing has completely disrupted the helium layer in model u225 and mixed it with the hydrogen envelope. The helium layer has also been mixed with the hydrogen envelope, although to a lesser extent, in model u200 and to an even slighter degree in model u250. These u-series models also experienced some mass loss due to pulsations.

The ρr^3 values through which the shock passes are an effective predictor of post-explosion hydrodynamics. In regions where ρr^3 increases, the shock must decelerate, and a reverse shock forms that inverts the pressure gradient and induces Rayleigh-Taylor (RT) instabilities. Models with steeper values of ρr^3 will experience more mixing because the forward shock slows down more abruptly, which leads to a stronger reverse shock. We show ρr^3 values for all models in Figure 1, scaled to the maximum value in model u225. It is clear from this figure that models u225 and u200 exhibit the largest increases in ρr^3 near the outer edge of the star. This is due to slight bumps in density that are connected to the pulsations that ejected mass from these stars earlier.

We show final states of mixing for the PISNe in Figure 2. The models are shown at different times, but always after the shock emerged from the surface of the star and the reverse shock, if one formed, dissipated. Density is shown on the left in each panel, with values scaled to the maximum and minimum densities in the simulation, while oxygen is shown on the right, with the values indicated in the color bar. Some similarities between the models exist across all stellar structures. In the higher-mass compact models (z225 and z250) and in the red u-series models above 150 solar masses, the bulk of the oxygen layer was swept up into a shell of higher density than the material on either side.

In general, however, the z-series explosions evolved quite differently than the u-series SNe. In the z-series, no reverse shock formed. A reverse shock formed in all the u-series models, but dissipated by the time it reached the density contrast at the oxygen layer (u150 and u175) or was too weak by the time it reached this dense shell to induce rapid RT growth (u250). In two models, a

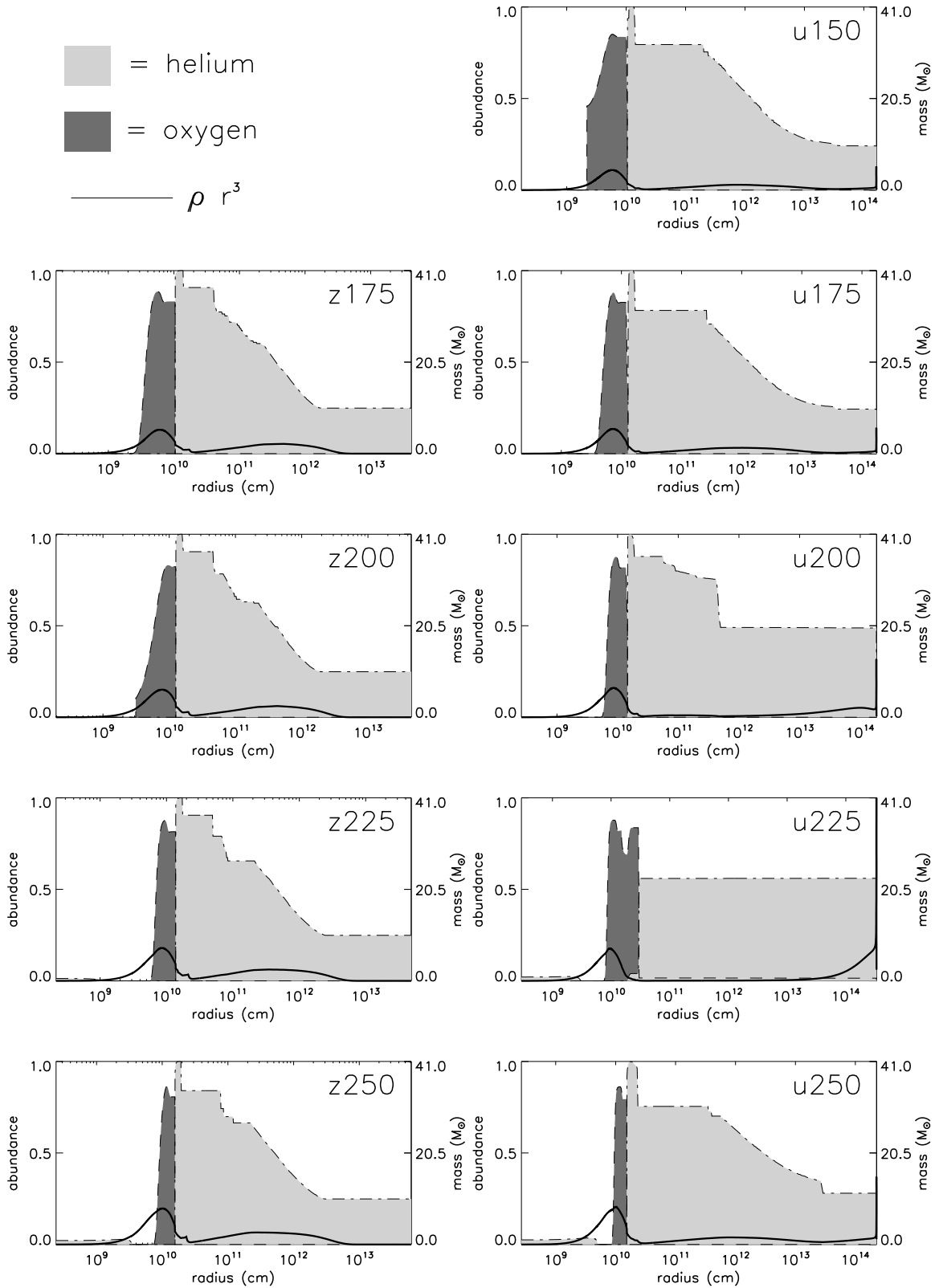


FIG. 1.— The structure of helium and oxygen shells (delineated by dashed lines for clarity) in all the progenitors, with ρr^3 superimposed on them. The ρr^3 profiles have all been scaled to the maximum ρr^3 in model u225. ρr^3 increases dramatically near the edge of some models that die as red giants, while none of the blue giants show a similar structure. The plateaus in helium abundance above cosmological values, which are most apparent in model u225, denote convective regions in which the hydrogen envelope mixed with a portion of the helium layer. This process completely disrupted the helium layer in model u225, and mixed a smaller fraction of the helium layer with the hydrogen envelope in model u200. A small amount of the helium shell convectively mixed with the hydrogen envelope in model u250.

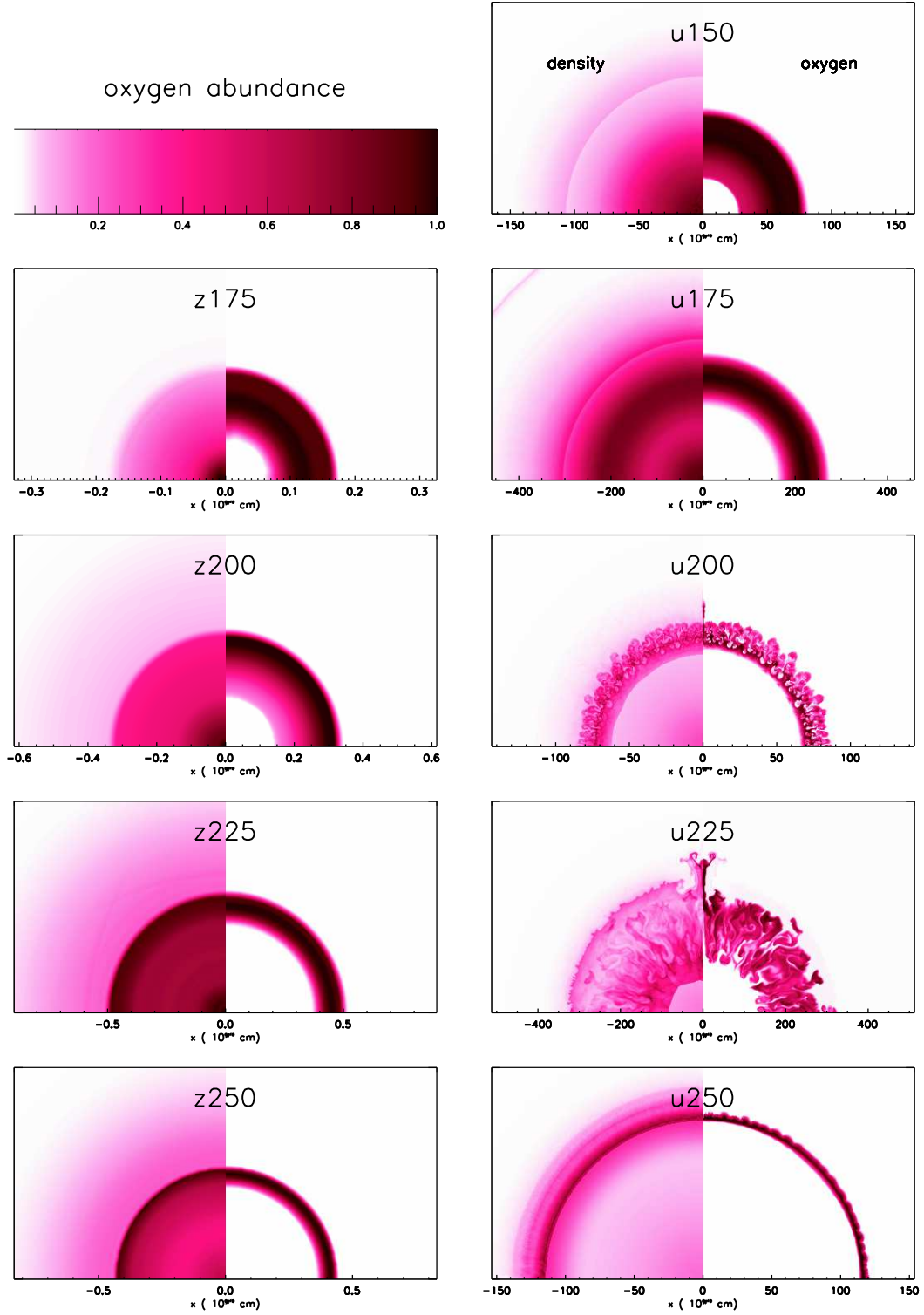


FIG. 2.— Images of density and oxygen abundance for all models after the forward shock exits the star or the reverse shock (if one forms) traverses the star, whichever is later. Density is scaled to the minimum and maximum values within a given simulation. A dense shell formed in all models with masses greater than $200 M_{\odot}$, but the RT instability only grows appreciably in the u200 and u225 models. These were the largest progenitors in radius and had the steepest ρr^3 curves. Only slight RT growth is evident in model u250.

reverse shock formed that was strong enough to drive rapid growth of RT instabilities (u200 and u225). The reverse shock was strongest in model u225, which had the steepest increase in ρr^3 and the second highest explosion energy, after model u250. The RT instability is clearly visible in the u200 and u225 panels in Figure 2. In these models the instability became nonlinear because individual RT fingers strongly interacted. In model u250, the RT instability only reached the early linear phase before its growth was halted.

The extent to which the structure of the PISN at the time of explosion was preserved or disrupted by mixing is shown in Figure 3. We plot the initial shell structure of the PISN at the time of mapping into CASTRO as a dashed line, and overlay a solid line indicating the abundances of these elements after the shock exited the star or the reverse shock traversed the star, whichever was later. The slight smoothing in the final profiles in comparison to the initial ones is due to numerical diffusion over the course of the simulation. The u200 and u225 panels demonstrate the extent of mixing in these explosions. The oxygen layer has been completely disrupted, and mixing has penetrated just to the top of the silicon layer (in u200) or through the silicon layer (in u225). The most vigorous mixing occurred in model u225, where hydrogen shell boost led to convection that completely mixed the helium shell and the hydrogen envelope. The only other models to experience RT mixing, models u200 and u250, are also the only other models that show evidence of convective mixing in the outer region of the star prior to explosion. Model u200 manifests more RT mixing and a larger region (in radius and mass) in which convection mixed part of the helium layer with the hydrogen envelope prior to explosion. Model u250, which has the smallest amount of convection extending into the helium layer, also exhibits the least RT growth. Models with no convective mixing between the helium layer and the hydrogen envelope manifest no RT mixing during the explosion, so mixing seems tied to the depth to which this convective envelope has penetrated the helium layer of the star. The deeper the convective envelope, the more RT mixing occurs during the supernova shock.

RT-induced mixing in PISNe, if it occurs at all, is unlikely to leave the remnant in a state that resembles a core-collapse supernova remnant. In particular, it is unlikely to dredge up significant amounts of oxygen, let alone silicon or ^{56}Ni , into the outer regions of the star, or draw much hydrogen back towards the center of the blast. The most vigorous mixing occurs in the model with the helium shell that has been completely disrupted by convective mixing with the hydrogen envelope, and likely represents the most mixing that can occur in a PISN. Even in this model, ^{56}Ni cannot reach the upper layers of lighter elements.

As noted earlier, our CASTRO simulations exclude the first stages of the explosion, in which oxygen burning drives convective mixing that may perturb the star (Chen et al. 2010). Since these perturbations are expected to be of low mode and high amplitude, it is unlikely they would alter the essential conclusions of our survey. Reprising our two-dimensional calculations in three dimensions is unlikely to yield significantly different results. The RT instability initially grows about 30% faster in three dimensions than in two because of ar-

tificial drag forces arising from two-dimensional geometries (Hammer et al. 2010). However, once the fingers of the instability begin to interact with one another, they mix more efficiently in three dimensions than in two, reducing the Atwood number and hence their growth rate (Joggerst et al. 2010b). These two effects cancel each other, and the width of the mixed region in two and three dimensions is the same. For spherical simulations like ours in which the RT fingers significantly interact, two-dimensional and three-dimensional simulations would exhibit comparable degrees of mixing. Also, the RT instability will not appear in three dimensions when it is not manifest in two.

4. DISCUSSION AND CONCLUSIONS

Unlike 15 - 40 M_{\odot} core-collapse Pop III SNe, 150 - 250 M_{\odot} Pop III PISNe experience either no internal mixing prior to shock breakout from surface of the star or only modest mixing between the O and He shells. Minor mixing occurs in only two of the explosions and is due to the formation of a reverse shock that is strong enough to trigger the RT instability at the dense shell created by the forward shock at the top of the oxygen layer. The degree of mixing is principally a function of how well hydrogen shell boost mixes the helium shell with the hydrogen envelope. The model in which the helium shell is completely mixed with the hydrogen envelope exhibits the most mixing. The general lack of internal mixing in PISNe has several consequences for early chemical enrichment of the IGM, the formation of second generation stars, and the observational signatures of such explosions.

First, the elements that are expelled by low-mass Pop III SNe (which are governed by both mixing and fallback onto the compact remnant) are later imprinted on new stars in essentially the proportions in which they are created by the explosions, regardless of how and where the stars form. This is because the metals are already highly mixed by the time the shock exits the star and are merely diluted upon further expansion into the halo and IGM, where new stars might form. This implies that IMF averages of nucleosynthetic yields of primordial core-collapse SNe can be directly compared to chemical abundances in ancient metal-poor stars, without regard for any intervening hydrodynamical processes. Indeed, the fact that elemental yields from Salpeter IMF averages of 15 - 40 M_{\odot} progenitors in JET10 match those found in two observational surveys of extremely metal-poor (EMP) stars suggests that the bulk of early chemical enrichment may have been due to low-mass Pop III stars. This is at odds with the current state of the art in Pop III star formation simulations, which suggest that the first stars were predominantly 100 - 500 M_{\odot} .

Determining the nucleosynthetic imprint of PISNe on second-generation stars is much more problematic because their metals may have differentially contaminated new stars. This is because metals in PISNe mixed with each other and with the surrounding IGM on much larger spatial scales, at radii where new stars may have formed. Except in models u200 and u225 at the interface of the O and He shells, and in model u225 at the interface of the O and Si shells, the shells of elements in the ejecta of other PISNe expand homologously until they sweep up their own mass in the ambient H II region, at radii of 10 - 15 pc. At this point, a reverse shock detaches from the

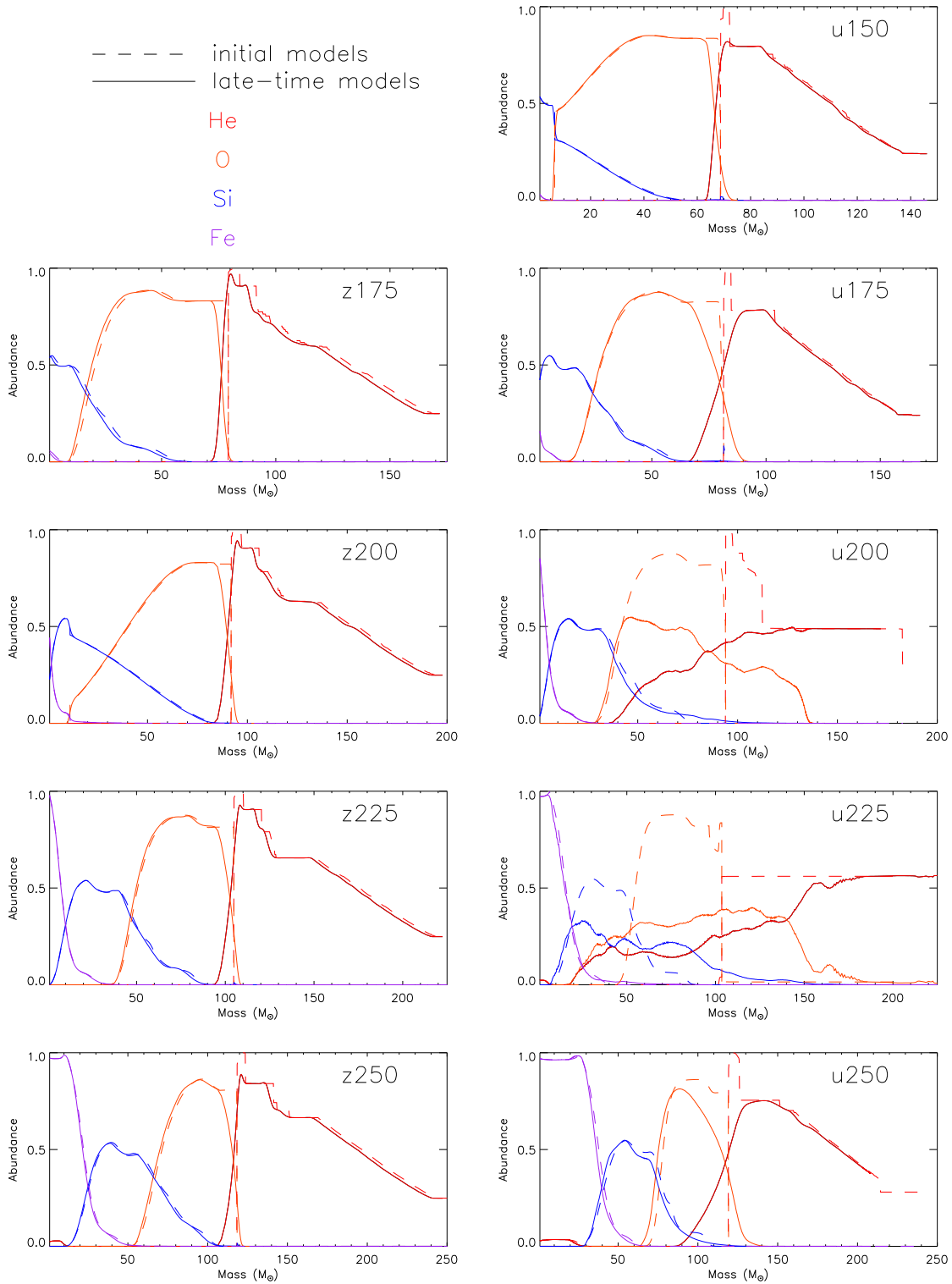


FIG. 3.— Initial and final abundances of He, O, Si, and Fe for all models. The RT instability is only present in models u200, u225, and to a small degree in u250. The slight disagreement between initial and final profiles for models which experienced no mixing is due to numerical diffusion over the evolution times of these models. In none of the mixed models did mixing break through the Si layer of the star, so ^{56}Ni never reaches the surface of the explosion as it does in core-collapse supernova explosions.

forward shock and a contact discontinuity forms between them (the Chevalier phase— Whalen et al. 2008). Both the reverse shock and contact discontinuity are prone to dynamical instabilities that will mix elements from the interior of the remnant with the surrounding medium. Later, on scales of 100 - 200 pc, further mixing will occur upon collision of the remnant with the dense shell of the relic H II region.

In this case, the elements that are taken up into new stars depends on how and where the stars form. If metals migrate out into cosmological flows and then fall back into the halo via accretion and mergers on timescales of 50 - 100 Myr, they likely will be well-mixed, with all elements formed in the explosion appearing in the new star (Greif et al. 2007; Wise & Abel 2008b; Greif et al. 2010). However, new stars may form at much earlier times in the SN remnant at radii where mixing takes place. One way this could happen is if metals at the interface between the ejecta and swept-up shell suffuse into and cool the shell, causing it to fragment into clumps that are unstable to gravitational collapse (e.g. Mackey et al. 2003). In this scenario, such clumps would be enriched only by the elements residing in the relatively narrow zone in which the stars form. This still does not explain why some hyper metal-poor stars have such high [C, N, and O/Fe] ratios. While C and O would be preferentially deposited on the clumps in which such stars form because they are predominant in the outer layers of the ejecta, PISNe do not produce enough N to account for measured abundances in these stars. However, little iron from deep in the interior of the remnant would reach the clumps because it is not mixed, which is consistent with the abundances measured in EMP stars to date. The failure to uncover the characteristic odd-even nucleosynthetic signature of PISNe predicted by Heger & Woosley (2002) metal-poor star surveys thus far has led some to suppose that primordial stars may not have been very massive, but it is possible that such signatures have been masked by observational selection effects (Karlsson et al. 2008). Unlike for low-mass stars, detailed numerical simulations that follow differential enrichment are required to determine the true chemical imprint of PISNe on second-generation stars.

Second, our results imply that, unlike in SN 1987A or low-mass Pop III SNe, Ni and Fe emission lines will not appear immediately after radiation breakout from the shock because there is not enough mixing to transport these elements out to the photosphere of the fireball. This may be key to distinguishing between Pop III core-collapse explosions and PISNe. The light curves of these supernovae are characterized by a sharp intense initial transient that decays over several hours into a dimmer extended plateau that persists for 2 - 3 months in core-collapse events and 2 - 3 years in PISNe (Fryer et al. 2010; Whalen & Fryer 2010). The initial pulse is powered by the thermal energy of the shock and the plateau is energized by radioactive decay of ^{56}Ni (the long life of the plateau is due to the longer radiation diffusion timescales through the massive ejecta). Preliminary ra-

diation hydrodynamical calculations of PISN light curves and spectra indicate that their peak bolometric luminosities are similar to those of Type Ia and core-collapse SNe, making determination of the mass of the progenitor from the magnitude of the initial transient problematic. If, however, Ni and Fe are detected just after radiation breakout, one can be confident that the explosion is due to a low-mass primordial star, and a Pop III IMF could begin to be built up by samples of such detections.

Our models also demonstrate that one-dimensional radiation hydrodynamical models are sufficient to capture most features of PISN light curves and spectra because the mixing such calculations exclude, which would alter the order in which emission lines appear over time, is minor. The picture for core-collapse Pop III SNe is quite different because vigorous mixing prior to the eruption of the shock from the surface of the star mandates its inclusion in light curve models. Two-dimensional multigroup radiation hydrodynamical calculations of such spectra lie within the realm of current petascale platforms, but a less costly approach can incorporate mixing in one-dimensional models. If most mixing in low-mass Pop III explosions occurs before radiation breaks free from the shock, two-dimensional models such as those in JET10 can be used to compute the distribution of elements in the ejecta just before breakout. These explosions can then be azimuthally averaged onto the one-dimensional grid of the light curve calculation and evolved to compute spectra. On average, along any given line of sight out of the SN, this method will produce emission lines in the likely order they would be observed.

These simulations, together with our previous survey of mixing and fallback in low-mass Pop III SNe, are the first of a numerical campaign to model the chemical enrichment of the early cosmos from its smallest relevant spatial scales. The eventual goal of this campaign is to understand the contribution of the first SNe to the formation of new stars and the assembly of primeval galaxies, which will soon be probed by the *James Webb Space Telescope (JWST)* and the *Atacama Large Millimeter Array (ALMA)*. The next stage of these numerical simulations will incorporate mixing on subparsec scales to determine if new stars directly form in the remnants of the first supernova explosions and follow their congregation into the first galaxies.

The authors thank Stan Woosley for helpful discussions and the use of his KEPLER progenitor models. CCJ was supported in part by the SciDAC Program under contract DE-FC02-06ER41438. DJW acknowledges support from the Bruce and Astrid McWilliams Center for Cosmology at Carnegie Mellon University. Work at LANL was done under the auspices of the National Nuclear Security Administration of the U.S. Department of Energy at Los Alamos National Laboratory under Contract No. DE-AC52-06NA25396. All simulations were performed on the open cluster Coyote at Los Alamos National Laboratory.

REFERENCES

- Abel, T., Bryan, G. L., & Norman, M. L. 2000, *ApJ*, 540, 39
 —. 2002, *Science*, 295, 93
 Abel, T., Wise, J. H., & Bryan, G. L. 2007, *ApJ*, 659, L87
 Almgren, A. S., Beckner, V. E., Bell, J. B., Day, M. S., Howell, L. H., Joggerst, C. C., Lijewski, M. J., Nonaka, A., Singer, M., & Zingale, M. 2010, *ApJ*, 715, 1221

- Alvarez, M. A., Bromm, V., & Shapiro, P. R. 2006, *ApJ*, 639, 621
- Beers, T. C. & Christlieb, N. 2005, *ARA&A*, 43, 531
- Bromm, V., Coppi, P. S., & Larson, R. B. 1999, *ApJ*, 527, L5
—, 2002, *ApJ*, 564, 23
- Bromm, V., Ferrara, A., Coppi, P. S., & Larson, R. B. 2001, *MNRAS*, 328, 969
- Bromm, V., Yoshida, N., & Hernquist, L. 2003, *ApJ*, 596, L135
- Chen, K., Heger, A., & Almgren, A. 2010, *ArXiv e-prints*
- Ekström, S., Meynet, G., Chiappini, C., Hirschi, R., & Maeder, A. 2008, *A&A*, 489, 685
- Frebel, A., Aoki, W., Christlieb, N., Ando, H., Asplund, M., Barklem, P. S., Beers, T. C., Eriksson, K., Fechner, C., Fujimoto, M. Y., Honda, S., Kajino, T., Minezaki, T., Nomoto, K., Norris, J. E., Ryan, S. G., Takada-Hidai, M., Tsangarides, S., & Yoshii, Y. 2005, *Nature*, 434, 871
- Fryer, C. L., Hungerford, A. L., & Rockefeller, G. 2007, *International Journal of Modern Physics D*, 16, 941
- Fryer, C. L., Whalen, D. J., & Frey, L. 2010, *ArXiv e-prints*
- Greif, T. H., Glover, S. C. O., Bromm, V., & Klessen, R. S. 2010, *ApJ*, 716, 510
- Greif, T. H., Johnson, J. L., Bromm, V., & Klessen, R. S. 2007, *ApJ*, 670, 1
- Hammer, N. J., Janka, H., & Müller, E. 2010, *ApJ*, 714, 1371
- Heger, A. & Woosley, S. E. 2002, *ApJ*, 567, 532
- Hirschi, R. 2007, *A&A*, 461, 571
- Iwamoto, N., Umeda, H., Tominaga, N., Nomoto, K., & Maeda, K. 2005, *Science*, 309, 451
- Joggerst, C. C., Almgren, A., Bell, J., Heger, A., Whalen, D., & Woosley, S. E. 2010a, *ApJ*, 709, 11
- Joggerst, C. C., Almgren, A., & Woosley, S. E. 2010b, *ArXiv e-prints*
- Joggerst, C. C., Woosley, S. E., & Heger, A. 2009, *ApJ*, 693, 1780
- Karlsson, T., Johnson, J. L., & Bromm, V. 2008, *ApJ*, 679, 6
- Kitayama, T. & Yoshida, N. 2005, *ApJ*, 630, 675
- Kitayama, T., Yoshida, N., Susa, H., & Umemura, M. 2004, *ApJ*, 613, 631
- Mackey, J., Bromm, V., & Hernquist, L. 2003, *ApJ*, 586, 1
- Nakamura, F. & Umemura, M. 2001, *ApJ*, 548, 19
- O’Shea, B. W. & Norman, M. L. 2007, *ApJ*, 654, 66
- Scannapieco, E., Madau, P., Woosley, S., Heger, A., & Ferrara, A. 2005, *ApJ*, 633, 1031
- Smith, B. D. & Sigurdsson, S. 2007, *ApJ*, 661, L5
- Weaver, T. A., Zimmerman, G. B., & Woosley, S. E. 1978, *ApJ*, 225, 1021
- Whalen, D., Abel, T., & Norman, M. L. 2004, *ApJ*, 610, 14
- Whalen, D., van Veelen, B., O’Shea, B. W., & Norman, M. L. 2008, *ApJ*, 682, 49
- Whalen, D. J. & Fryer, C. 2010, *ArXiv e-prints*
- Wise, J. H. & Abel, T. 2008a, *ApJ*, 684, 1
- , 2008b, *ApJ*, 685, 40
- Woosley, S. E., Heger, A., & Weaver, T. A. 2002, *Reviews of Modern Physics*, 74, 1015